Acta Geotechnica (2007) 2:269–279
DOI 10.1007/s11440-007-0045-9

RESEARCH PAPER

Three-dimensional petrographical investigations on borehole rock samples: a comparison between X-ray computed- and neutron tomography

P. Christe · M. Bernasconi · P. Vontobel · P. Turberg · A. Parriaux

Received: 20 October 2006 / Accepted: 4 October 2007 / Published online: 17 November 2007

Abstract Technical difficulties associated with excavation works in tectonized geological settings are frequent. They comprise instantaneous and/or delayed convergence, sudden collapse of gallery roof and/or walls, outpouring of fault-filling materials and water inflows. These phenomena have a negative impact on construction sites and their safety. In order to optimize project success, preliminary studies on the reliability of rock material found on site are needed. This implies in situ investigations (surface mapping, prospective drilling, waterflow survey, etc.) as well as laboratory investigations on rock samples (permeability determination, moisture and water content, mineralogy, petrography, geochemistry, mechanical deformation tests, etc.). A set of multiple parameters are then recorded which permit better insight on site conditions and probable behavior during excavation. Because rock formations are by nature heterogeneous, many uncertainties remain when extrapolating large-scale behavior of the rock mass from analyses of samples order of magnitudes smaller. Indirect large-scale field investigations (e.g. geophysical prospecting) could help to better constrain the relationships between lithologies at depth. At a much smaller scale, indirect analytical methods are becoming more widely used for material investigations. We discuss in this paper X-ray computed tomography (XRCT) and neutron tomography (NT), showing promising results for 3D petrographical investigations of the internal structure of opaque materials. Both techniques record contrasts inside a sample, which can be interpreted and quantified in terms of heterogeneity. This approach has the advantage of combining genetic parameters (physico-chemical rock composition) with geometric parameters resulting from alteration or deformation processes (texture and structure). A critical analysis of such 3D analyses together with the results of mechanical tests could improve predictions of short- and long-term behavior of a rock unit. Indirect methods have the advantage of being non-destructive. However, as it is the case with large-scale geophysical surveying, XRCT and NT are affected by several error factors inherent to the interaction of a radiation modality (X-ray or neutron beam) with the atomic structure of the investigated materials. Recorded signals are therefore in particular cases not artifact-free and need to be corrected in a subsequent stage of data processing.

Keywords Geotechnical sample sizes · Neutron tomography · Petrographical investigations · Structure · Texture · X-ray computed tomography

P. Christe (✉) · P. Turberg · A. Parriaux
Laboratoire de Géologie de l'Ingénieur et de l'Environnement, Ecole Polytechnique Fédérale, Lausanne, Switzerland
e-mail: pierre.christe@epfl.ch

M. Bernasconi
Service de radiodiagnostic et radiologie interventionnelle, Centre Hospitalier Universitaire Vaudois, Lausanne, Switzerland

P. Vontobel
Spallation Neutron Source Division, ASQ, Paul Scherrer Institut, Villigen, Switzerland

1 Introduction

In the framework of a PhD project at EPFL, rock samples derived from recognition drilling were studied in order to investigate possible relationships between their geological and mechanical properties. This approach follows previous work by Bürgi [2, 3] and Habimana [6, 7]. It was found that geological parameters regrouped under a quality index called MSI (Mineralogical and Structural Index [2]) show

an apparent tendency to positively correlate with rupture values from triaxial compression [6]. Observations were made on quartzo-phyllitic rock samples from the Cleuzon-Dixence dam project in Switzerland. Conclusions of this research are encouraging but further work is needed to get more reliable results. The current research project seeks therefore to test the proposed methodology for rocks of varying petrological content.

A major problem pointed out by Bürgi [2] is the 2D nature of their petrographical and structural analysis. Until recently, the majority of microstructural investigations on rock samples were made by thin sections under a crossed-polarized microscope. The geometrical relevance of such investigations can be improved using new techniques that have become available to earth scientists that allow 3D visualization of the rock interiors. Computed tomographic methods have been applied for several years to different research projects in the earth science community (e.g. [4, 5, 9, 12, 15, 17, 18]). Performing a mineralogical and structural analysis of rock samples on the basis of 3D petrographical and petrological evidence could therefore considerably increase the relevance of a characterization procedure of the type envisaged by Bürgi et al. [3].

Although there is no doubt that non-destructive techniques are powerful, they do not represent an investigation standard in the field of engineering geology and they are still expensive. Beam flux intensities for a particular investigation must be high enough to penetrate dense materials and provide reliable measurement statistics. Submillimeter resolution investigations are therefore often only possible on small samples in the order of 2 × 2 cm, for which desktop scanners have become easily available (see for example at http://www.skyscan.be). Specialized centers working on new techniques for indirect 3D rock imaging report today resolutions of up to 1/1,000 of object diameter on samples up to about 8 cm in diameter with 200–225 kV microfocal X-ray sources; specific higher-energy instruments providing beam energy of 420–450 kV have somewhat lower spatial resolution but nevertheless permit high-quality micro-analysis on decimeter-scale samples (see UTCT, University of Texas at Austin, USA). Breakthrough resolution for indirect rock visualization is obtained with synchrotron derived irradiation sources that are characterized by high brightness and high intensity, many orders of magnitude more than with X-rays produced in conventional X-ray tubes. Reports from experiments performed at such facilities indicate today resolution potentials close to the nanometer scale (see European Synchrotron Radiation Facility, Grenoble, France).

Samples tested in this study are cylindrical probes from geotechnical reconnaissance drilling and have dimensions of about 8 × 16 cm. Rock cores collected in such operations are often fragile when extracted in difficult geological settings (see for example many drilling operations performed at the AlpTransit tunnelling sites in Switzerland, where cataclastic and kakiritic materials were frequently encountered) and require that there be minimal manipulation to preserve their structures and textures. Therefore, to keep a maximum of information from such rock samples, their initial shape and dimension are fixed parameters in indirect analysis aiming derivation of relevant 3D relationships at the represented scale to be combined with regional structural data. The samples presented hereafter were chosen for their contrasting petrological characters and for evaluating the potential of two irradiation techniques providing adequate beam flux intensities and energies for proper penetration of geotechnical rock core sizes. The first was the X-ray computed tomography facility found at the Radiodiagnostic Institute of the University Hospital in Lausanne (CHUV). Second, a neutron tomography station located at the Paul Scherrer Institute in Villigen (PSI) offered the possibility to perform tests on referenced materials. We present in this study observations made by both techniques on the same reference geotechnical samples. 3D reconstructed models will be presented as well as individual tomographic slices and the complementary nature of the two methods will be highlighted.

2 Presentation of rock samples

Four samples were chosen according to their contrasting structural characteristics as well as on their varying mineralogical compositions. Three samples were rock cylinders from reconnaissance drilling performed at the TRIDEL gallery site under construction in Lausanne that were tested at the EPFL under uniaxial compression (e.g. showing important fracturing). The last sample was drilled during field work near Vallorbe in the Jura Mountains. We present a short description of each sample:

2.1 CT1-co

CT1-co is a sample of reinforced concrete from the upper part of a drillhole at the TRIDEL site in Lausanne. Diameter of core is 84.5 mm and length is 160 mm. The clastic nature of concrete (aggregate) and the metallic iron fibers are easily recognized by eye in hand specimen. The sample was fractured under uniaxial compression at the Laboratory of Rock Mechanics of the EPFL (LMR) and gave resistance value of $\sigma_c = 30$ MPa.

Sample composition is a standard concrete of gravel and sand from Lausanne area, cement and a water content of about 35%.

2.2 CT2-sa

CT2-sa is a sample of medium-grained sandstone from the Lausanne grey molasse formation taken during drilling operation at the TRIDEL site in Lausanne. Sample diameter is 80 mm and length is 160 mm. Fracture testing under uniaxial compression at the LMR gave a peak resistance value of $\sigma_c = 9$ MPa. Fracture networks are recognizable on the outer surface of the sample.

Sandstone composition is about 40% detrital quartz, 20% $CaCO_3$, and smaller proportions of feldspar, Fe–Mg–, and micaceous minerals with structural formulas of type $(K,Na,Ca)_2(Al,Mg,Fe,Ti)_{4-6}(Si,Al)_8O_{20}(OH,F)_4$.

2.3 CT3-ma

CT3-ma is a sample of tectonized marl from a further reconnaissance drilling at TRIDEL site, Lausanne. Marls have a high proportion of clay minerals and tend to be very fine-grained. Moreover clays have a strong geotechnical meaning as they can capture water into their mineralogical structure allowing a strong swelling potential in case where smectite is present causing with time potential damage on geotechnical structures. Diameter of sample is 82 mm and length is 160 mm. Sample was fractured under uniaxial compression at the LMR and broke at $\sigma_c = 3.7$ MPa. Irregular surface shape and decompression fractures due to drying processes at the contact with ambient air affect the sample.

Marl composition is about 17% SiO_2, 43% CaO and 35% H_2O at saturation with minor proportions of Al_2O_3, Fe_2O_3, MgO, K_2O and Na_2O.

2.4 CT4-li

CT4-li is a tectonically fractured micritic limestone of Jurassic age collected along the Pontarlier fault zone near Vallorbe, in the Jura Mountains. Sample diameter is 76 mm and length is approximately 200 mm with irregular bases. Uniaxial resistance performed on a 55 mm wide sample from the same formation gave a σ_c value of 60 MPa. A set of fractures that are partly recrystallized with calcite, partly filled with clay materials, is visible by eye.

Limestone composition is about 80% $CaCO_3$, 2% H_2O and minor proportions of SiO_2, Al_2O_3, MgO, K_2O, Na_2O and FeO.

3 Analytical principles and methods

Tomography refers to the cross-sectional imaging of an opaque object from either transmission or reflection data collected by illuminating the object from different directions using a particular radiation modality (here either X-rays or neutrons). Recording of intensity signals from different projections angles (e.g. sinograms) and combination of these projections all together allows the reconstruction of a 3D tomographic image of the investigated structure. In the strict sense of the word, a projection at a given angle is the negative logarithmic transmission image in the direction specified by that angle, what can be expressed as the object internal properties derived from the transmitted intensities. The conversion of intensity signals into an image requires reconstructing a function from its projections. This can be achieved with the use of so-called convolution-backprojection algorithms [8, 13, 14].

Tomographic methods are based on attenuation measurements of an incident beam intensity through a material of a given composition. The recorded final intensity I is related to the initial intensity I_o through a linear attenuation coefficient defined as μ in the case of X-rays or as Σ in the case of thermal neutrons. Beer's Law, relating I to I_o, is expressed for a homogeneous material as follows:

$$I_{(x)} = I_o e^{-\mu x} = I_o e^{-\sum x}.$$

The physical properties of the source radiation control the interaction that will result with the atomic structure of the investigated material. X-rays are emitted as a polychromatic beam (i.e. containing a spectrum of energies) and interact mainly with the electron shells of atoms. This leads to a CT map of linear attenuation coefficients that are dependent on material density, element composition and radiation energy. A CT scan detects in that sense density and chemical contrasts between adjacent components. Energy dependent total linear X-ray attenuation coefficients μ including photon absorption and scattering can be derived from tabulated X-ray mass attenuation coefficients μ/ρ from, e.g. http://physics.nist.gov/PhysRefData/XrayMassCoef/cover.html by multiplying with material density ρ.

In NT polychromatic neutrons interact with the nucleus of an atom. Scattering and absorption effects in NT are therefore a function of the effective cross sectional area that an atom of a specific isotope presents to a given neutron flux. In that sense, neutrons are very sensitive to detection of light elements like hydrogen, boron or lithium, meaning that such elements present big neutron cross-sections and are therefore very attenuating. Contrary to X-rays, neutrons will penetrate dense materials with minimal attenuation. Although XRCT and NT differ in their detection potential, they are complementary methods in the sense that each technique will have advantages for a given detection purpose. As a rule of thumb, however, one can keep in mind that elements with similar atomic number Z

are better discriminated by neutrons than by X-rays. Table 1 is a list of common chemical elements found in rocks for which X-ray and neutron properties are listed together with solid state densities, atomic number and atomic weight.

As expressed before, 3D investigations of a structure are achieved by combining different radiation paths taken under different incremental angular projections using tomographic reconstruction algorithms. Acquisition is achieved by placing the sample on a rotary table rotating in small angular steps over 180° in the case of parallel beam projection in NT. For our XRCT measurements, sample orientation remains fixed while the source rotates over 360° around the sample placed on a table moving through the gantry, resulting in continuous helical data acquisition.

Final beam intensities are recorded on highly sensitive detectors specially designed for X-ray or neutron detection. They capture the 2D ray field perpendicular to the ray path. The geometry of the detector system must be appropriate in order to catch the entire rays. Scattering effects must be minimized in the case of NT due to device design (optimization between distance of sample from source and distance to detector). Signal records are finally converted in a slice image via the above mentioned convolution-back-projection algorithms.

Table 2 presents common rock-forming minerals classified by density for which linear attenuation coefficients were calculated for both XRCT and NT irradiations. Figure 1 makes a graphical comparison of these different attenuation coefficients and highlights the specific behavior of hydrated phases that are strongly opaque under NT investigation.

In the following we present the facilities we have used for XRCT and NT investigations.

3.1 X-ray computed tomography (XRCT)

XRCT measurements were performed at the University Hospital in Lausanne (CHUV) at the radiodiagnostic institute. CT scans were performed using a LightSpeed VCT from GE Medical Systems (http://www.gehealthcare.com). Detector is a 40 mm-wide HiLight® Matrix III Scintillator with isotropic design. It contains 64-channel detector rows made of 58,368 cells (912 detectors per row) with a thickness in the z-direction of 0.625 mm each, providing an isotropic resolution of 0.35 mm. Lighting angle of the detector is 56 degrees. Dynamic range is 16 bit and reconstructed density maps are 512 × 512 pixels. X-ray parameters were set to 120 kVp voltage and 640 mA tube current for a focal spot size of 1.2 mm. Acquisition was achieved in a helical mode corresponding to a continuous rotation of the CT gantry (X-ray source and detector) during the displacement of the sample at a constant speed of 25.8 mm/s. A full rotation was performed in 0.8 s and image reconstruction step was set to 0.3 mm providing a voxel size of 0.3 × 0.215 × 0.215. A reconstruction algorithm with a medium edge enhancement effect was used (DETAIL CT algorithm from GE Medical Systems).

Table 1 List of common chemical elements found in rocks for which total scattering and attenuation properties under X-ray and neutron irradiations are given, together with atomic number, atomic weight and solid state densities

Chemical element	Atomic number	Atomic weight (g mol^{-1})	Density (g cm^{-3})	X-ray mass attenuation coefficient (cm^2 g^{-1}) 120 keV	X-ray attenuation coefficient (cm^{-1}) 120 keV	Neutron scattering cross section (cm^2 g^{-1}) 1.8 Å, 25 meV	Neutrons attenuation coefficient (cm^{-1}) 1.8 Å, 25 meV
H	1	1.0079	0.09	0.282	0.025	49.013	4.411
C	6	12.011	2.26	0.144	0.325	0.278	0.629
O	8	15.999	1.43	0.146	0.209	0.159	0.228
Na	11	22.99	0.97	0.146	0.142	0.086	0.083
Mg	12	24.305	1.74	0.154	0.268	0.092	0.160
Al	13	26.982	2.7	0.153	0.413	0.034	0.091
Si	14	28.086	2.33	0.163	0.380	0.046	0.112
S	16	32.066	2.07	0.174	0.360	0.019	0.040
K	19	39.098	0.86	0.191	0.164	0.030	0.026
Ca	20	40.078	1.55	0.206	0.319	0.043	0.066
Ti	22	47.867	4.54	0.210	0.953	0.055	0.248
Fe	26	55.845	7.87	0.269	2.117	0.125	0.986

Note that the level of the irradiation energy strongly differs between the X-ray (120 keV) and the neutron data (25 meV), but correspond to effective scan parameters for each technique. X-ray mass attenuation coefficients taken from http://physics.nist.gov/PhysRefData/Xcom/html/xcom1.html [1] and total neutron cross sections calculated for a wavelength of 1.8 Å corresponding to a thermal neutron energy of 25 meV from http://www.ncnr.nist.gov/resources/n-lengths/list.html [16]. Attenuation coefficients include both coherent and incoherent scattering and absorption

Table 2 Calculated attenuation coefficients for relevant mineral species present in the studied samples and classified by density

Compound	Chemical formula	Density (g cm^{-3})	X-ray linear attenuation coefficient (cm^{-1}) 120 keV	Neutrons attenuation coefficient (cm^{-1}) 1.8 Å, 25 meV
Air	O_2	0.00	0.00000	0.00000
Water	H_2O	1.00	0.16100	5.38000
Microcline	$KAlSi_3O_8$	2.56	0.40448	0.24275
Kaolinite	$Al_2Si_2O_5(OH)_4$	2.60	0.39780	2.26568
Albite	$NaAlSi_3O_8$	2.62	0.39824	0.27165
Quartz	SiO_2	2.65	0.40810	0.28241
Chlorite	$(Mg,Fe,Al)_{12}[(Si,Al)_8O_{20}](OH)_{16}$	2.65	0.49555	1.16772
Smectite	$(Na,Ca)Al_4[(Si,Al)_8O_{20}](OH)_4{\cdot}2(H_2O)$	2.70	0.41850	1.26832
Calcite	$CaCO_3$	2.71	0.46070	0.34373
Illite	(K,H_3O) $[(Si,Al)_3O_{10}](OH)_2$	2.75	0.43175	1.89746
Anorthite	$CaAl_2Si_2O_8$	2.76	0.44160	0.26307
Muscovite	$KAl_3Si_3O_{10}(OH)_2$	2.83	0.44148	0.97482
Rutile	TiO_2	4.25	0.78625	0.41071
Ilmenite	$FeTiO_3$	4.79	1.01548	0.54514
Pyrite	FeS_2	5.01	1.09218	0.34386
Magnetite	Fe_3O_4	5.20	1.22200	0.70055
Hematite	Fe_2O_3	5.30	1.22960	0.71837

Structural formulas are given for each compound. X-ray attenuation coefficients for energies of 120 keV, neutrons attenuation coefficients for a wavelength of 1.8 Å corresponding to a thermal energy of 25 meV

In order to minimize beam hardening effects (preferential attenuation of low-intensity X-rays by crossing the sample due to the polychromatic nature of the X-ray beam) a sample holder made from a Cu-sheet surrounding a 2 cm thick PVC cylinder was used to pre-filter X-rays before entering the sample.

3.2 Neutron tomography (NT)

NT measurements were performed at the Paul Scherrer Institute (PSI) in Villigen at the Neutron Transmissions Radiography Station (NEUTRA, [10, 11]). Neutrons are generated at PSI through a proton accelerator by sending a 590 MeV proton beam at a target of heavy metal (lead). From there neutrons are ejected in a moderator tank and slowed down to thermal energy of approximately 25 meV ("SINQ", Swiss Spallation Neutron Source). Extraction of neutrons for radiographic and tomographic use is made through a flight tube forming a collimator that bundles neutron rays to a slightly divergent beam of about 35 cm diameter that is directed to the sample holder. Attenuated neutrons are then recorded on a 0.25 mm thick ^{6}Li-doped ZnS based neutron scintillator screen and imaged with a 1,024 × 1,024 pixel CCD camera. Acquisition times lasted 1.5 h (300 angular projections over 0.6° increments, 18 s

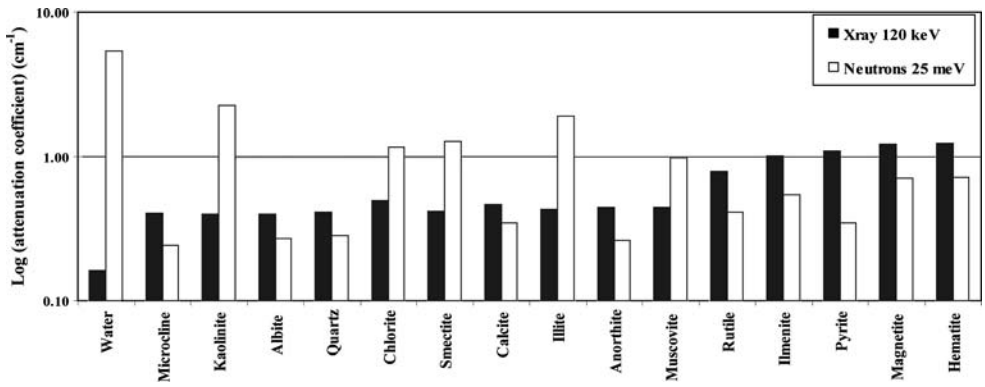

Fig. 1 Graphic presentation of the linear attenuation coefficients for X-rays (120 keV) and neutrons (1.8 Å and 25 meV) for the mineral species listed in Table 2. Clay minerals and hydrated mineral species become particularly well highlighted in the neutron data

illuminations for each view). Three additional exposures without sample (flatfield views) and one exposure without neutron beam (CCD noise background) were taken. These are used to derive the transmission values I/I_o from the sample projection images.

Rock samples were placed at position 2 of NEUTRA providing a collimation ratio L/D of 350 and a field of view of 97 × 97 mm using a 50 mm objective (Pentax 50 mm F 1.2). Neutron flux is 5.0×10^{-6} cm^{-2} s^{-1} per mA. Nominal resolution is 0.095 mm per pixel (0.215 mm per pixel in the case of XRCT). Geometric distortion due to distance from sample to scintillator was evaluated to be 0.143 mm.

Due to the size of the rock samples only about one half of their volume could be visualized at NEUTRA (300 images), as opposed to the 560 images encompassing the entire volumes acquired via XRCT.

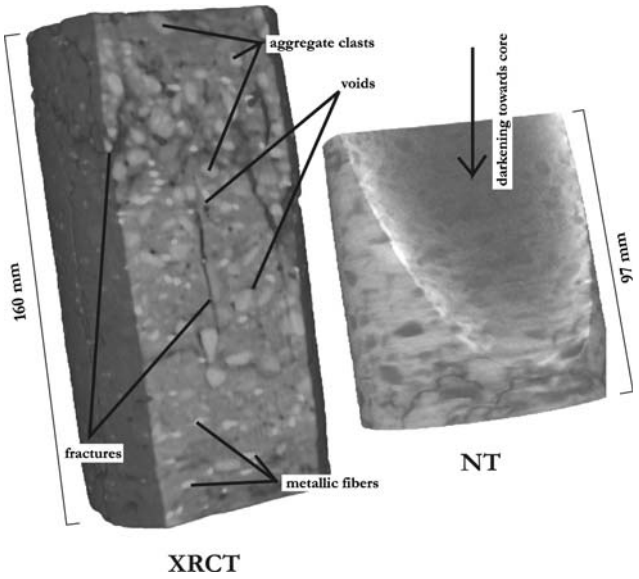

Fig. 2 XRCT (*left*) and NT (*right*) 3D reconstructions of fractured sample CT1-co. Main features of sample are pointed out on the XRCT model. Note decreasing recorded information towards the core of sample CT1-co in the NT image, as indicated by a shadow zone (*arrow*)

4 Results and discussion

XRCT and NT data were edited at NEUTRA with the help of VGStudio MAX software (http://www.volumegraphics.com) for voxel data visualization and analysis. 2D visualizations of individual tomographic "slices" were performed with the freeware ImageJ^{TM} (rsb.info.nih.gov/ij).

Quality and displayed contrasts differ strongly between both methods. Table 2 presents comparative attenuation coefficients for X-rays and thermal neutrons for the typical mineral species found in the four rock samples CT1-co, CT2-sa, CT3-ma and CT4-li.

Sample CT1-co is representative of a clastic texture where individual components can be visualized in a cement matrix. This type of material can be seen as a bimodal structure, where matrix properties will have a strong influence at the early stage of any deformation process before clast deformation will initiate. Recognition of fractures or voids in the matrix is therefore crucial to better characterize a deformation process, as well as clast shapes. The XRCT model of CT1-co provides good 3D information on the entire sample thickness whereas discrimination of individual particles is only possible by means of NT investigations on a peripheral area. This is probably due to the amount of hydrated components present in the matrix cement used for concrete preparation but also on an inappropriate sample size for proper neutron penetration in such materials (Fig. 2).

Decimeter-scale concrete is therefore too attenuating for neutrons to penetrate properly. The high hydrogen content in concrete leads to a low neutron transmission. The high scattering probability of neutrons induces additional blurring and a strong deviation from the exponential attenuation law.

On the contrary, densities of aggregate components and hydrated cement are in a good range for X-ray penetration for the given sample size. The 1 mm bright metallic fibers used in this concrete type for enhanced mechanical performance are displayed with a strong saturation level on XRCT images whereas they are practically invisible on NT images (Fig. 3). Fractures present in sample CT1-co are only discernable on the outlines of the NT model, whereas they are strongly contrasting in the internal parts of the XRCT model (Fig. 3).

Sample CT2-sa is homogeneous mid-grained sandstone with grain sizes in the millimeter to submillimeter range. Grain packing in the matrix is therefore only slightly visible on XRCT or NT scans as we get close to the limits of resolution of both techniques. Sample CT2-sa is interesting in terms of differentiation between rock matrix and fracture patterns. The sandstone is mainly composed of detrital quartz and feldspar grains for which X-rays and neutrons attenuation coefficients are quite similar (Table 2). The porous nature of sandstone permits only little water to remain in the rock structure if material has time to dry under ambient air conditions. Therefore, neutron penetration in CT2-sa is about as good as in the case of X-rays (Fig. 4).

Structures of interest like fractures offer good contrasts with both methods. Figure 5 shows a 3D reconstruction from the NT scan. Fracture outlines are similarly detected with XRCT (Fig. 4). Sample CT2-sa is therefore representative of a material that is productively investigated with both methods.

Sample CT3-ma is a material that is in between a rock and a soil ("soft rock-hard soil"). It has a plastic

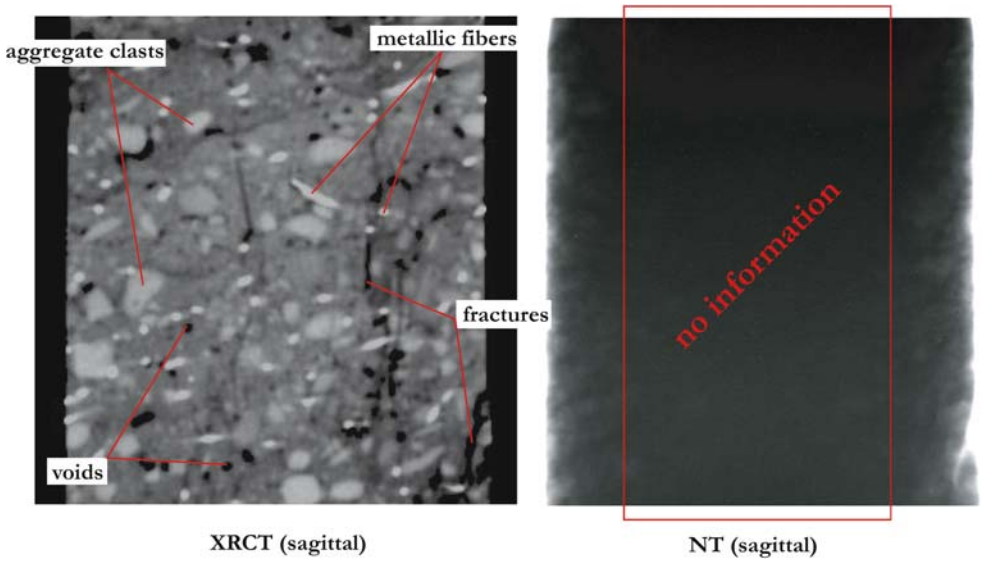

Fig. 3 Individual sagittal XRCT (*left*) and NT (*right*) slices of fractured sample CT1-co. Due to the limited field of view of our NT instrument only about 70% of sample length is presented here. Different components are pointed on the XRCT picture. The NT slice is poorly resolved in the internal sample parts due to inappropriate sample dimensions for neutron penetration and the presence of hydrated species in the cement matrix

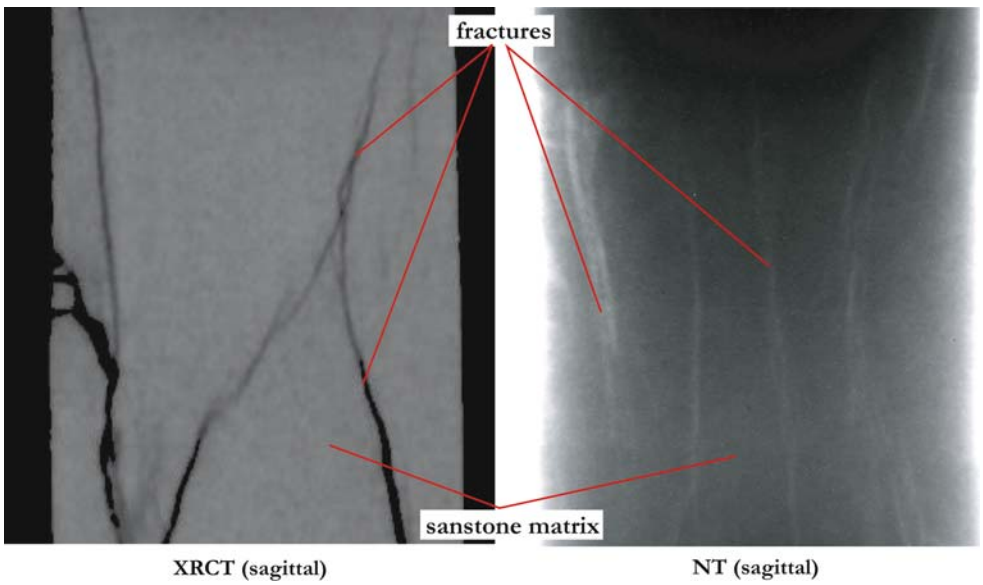

Fig. 4 Comparative sagittal XRCT and NT slices of fractured sample CT2-sa. In the case of dry sandstone, neutron penetration is achieved across the entire sample thickness and gives result in good concordance with XRCT visualization

mechanical behavior that is controlled by important proportions of clay minerals and by the effective water content of the sample. In such materials, void features like fractures will tend to seal easily when wet, implying a very low permeability. However, crack patterns caused by decompression will form when the material is submitted to a drying process. The fractures visible on the surface of sample CT3-ma result from prolonged contact with ambient air contracted during storage after completion of the uniaxial compression test.

The significant abundance of hydrated mineral species like clays makes any neutron radiography or tomography on such materials inefficient for large samples (Table 2; Fig. 6). Investigations of the inside parts of the sample are instead possible with X-rays. The very fine-grained nature of such marls is however a big problem for the resolution

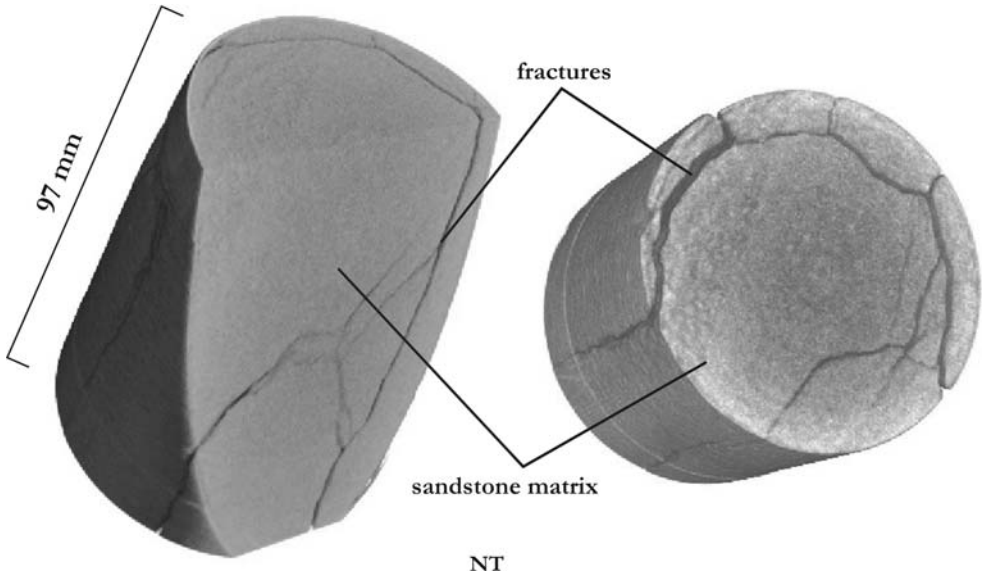

Fig. 5 Reconstructed NT models of fractured sample CT2-sa. As the rock matrix is very homogeneous, features like fractures are highly contrasting and easily detected in a tomographic image

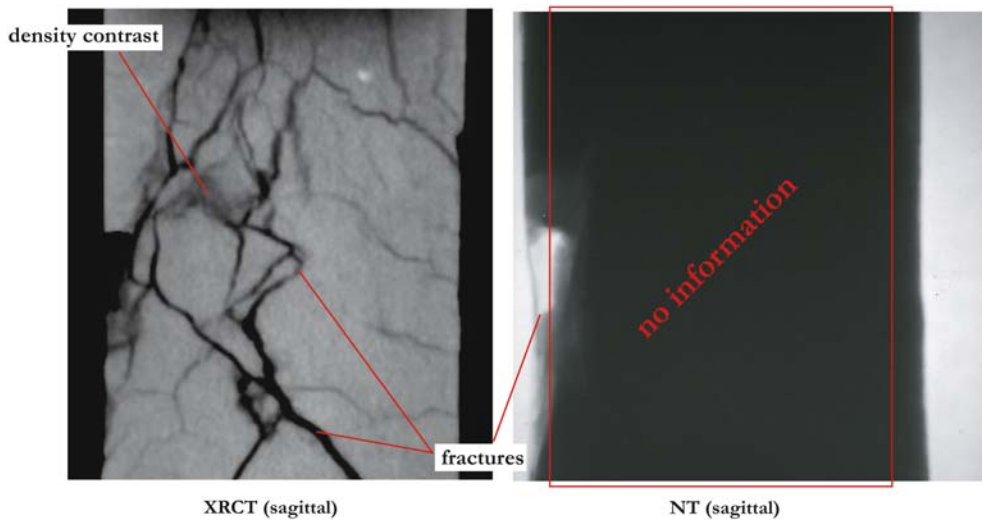

Fig. 6 Comparative sagittal XRCT (*left*) and NT slices (*right*) of fractured sample CT3-ma. Neutron penetration is very poor due to significant quantity of hydrated mineral species inside the sample as well as sample dimensions

of features of interests other than penetrative fractures. CT slices show however regions of contrasting densities reflecting a probable modification of the internal structure of the sample that could eventually be linked to alteration processes (increase in overall microporosity, Fig. 6). Reconstructed NT images were compared with the XRCT scan on a broken surface at the sample outline. The NT model is strongly blurred compared to the XRCT model according to detection of fine fractures but renders the general core shape accurately (Fig. 7).

Sample CT3-ma is therefore characterized as an extreme material where both methods run up against some detection limits. However, individual CT slices reflecting density contrasts related to alteration states and/or material heterogeneities present the possibility of detecting mechanically important features that would remain hidden by classical investigation techniques.

Clays are on the other hand an interesting contrasting agent for NT detection if only present in small proportions inside a sample. As for the case of sample CT4-li, which represents again a homogeneous rock matrix separated by different cracks, structures like clay-filled fractures are very nicely displayed on an NT model (Fig. 8). The entire limestone matrix appears quite transparent to neutrons but

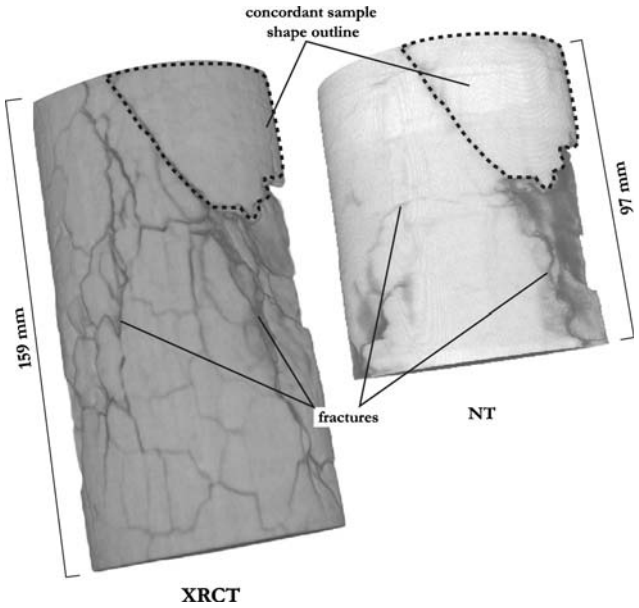

Fig. 7 3D models reconstructed for fractured sample CT3-ma. Left is an XRCT view and right the poorly resolved NT view. Both techniques give concordant results in the visualization of the *broken outline* of the sample represented by a *dashed surface area*. However, resolution of fractures patterns due to drying of the sample at ambient air is poorly realized in the case of NT investigation

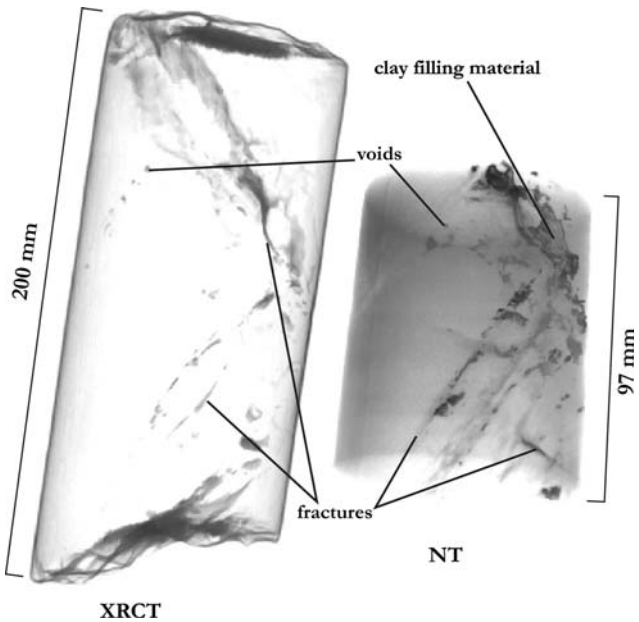

Fig. 8 3D models of sample CT4-li. NT reconstruction (right) permits nice visualization of clay materials inside cracks (*dark grey spots*) and displays with better contrast than XRCT a presumed fracture patterns inside the sample

clays in small proportions give a very high contrast on NT scans due to the amount of bounded water present in the mineralogical structure (Fig. 8). This is apparently better achieved with NT than with XRCT but would need to be properly quantified.

Fracturing of limestones under tectonic processes involves circulation of calcite-enriched fluids. These fluids will preferentially precipitate inside open cracks and will eventually seal the existing fractures modifying their mechanical properties. Because of identical densities between precipitating calcite and limestone matrix, these features will tend to become invisible by XRCT investigation. NT scans are apparently more promising for the detection of such sealed fractures (Fig. 9).

For a geomechanical interpretation it is indeed important to detect such features as they could influence the whole mechanical behavior of a rock sample.

5 Conclusions

In the case of samples of similar shapes and size, as it is the case for this study, a direct comparison of X-ray Computed- and Neutron Tomography can be achieved. Differences in image contrasts result primarily from different attenuation properties of X-rays and neutrons by crossing a given material but also from optimization of the device parameter settings for a particular investigation (irradiation time, X-ray voltage and beam focal spot size, sample distance from neutron source, etc.). Although not especially designed for our investigation purpose, a rapid access to the two techniques could be obtained at a medical XRCT facility and at a NT facility providing test measurement opportunities. XRCT and NT were therefore applied in order to qualitatively determine which technique would better permit a rapid 3D imagery of quality that could be integrated in the process of rock mass characterization during geotechnical reconnaissance drilling operations. Prerequisites were to keep the rock core sizes unmodified (implying adequate parametrization of the XRCT and NT scanners to reach a penetration depth of <10 cm) and to get a resolution potential precise enough to highlight geological relevant features for a geomechanical 3D analysis. In that sense, XRCT seems to be more versatile than NT for producing imagery of interest independent of the petrological type of the analyzed sample. NT however, has some advantages when small proportions of the volume like clay-filling materials must be tracked precisely. The strong attenuation induced by hydrated species provides a contrast of high-quality on NT scans that looks more precise than on comparative XRCT-scans. Different interactions of these two irradiation modalities with a material of given composition mean that the two techniques could be used as complimentary analytical methods.

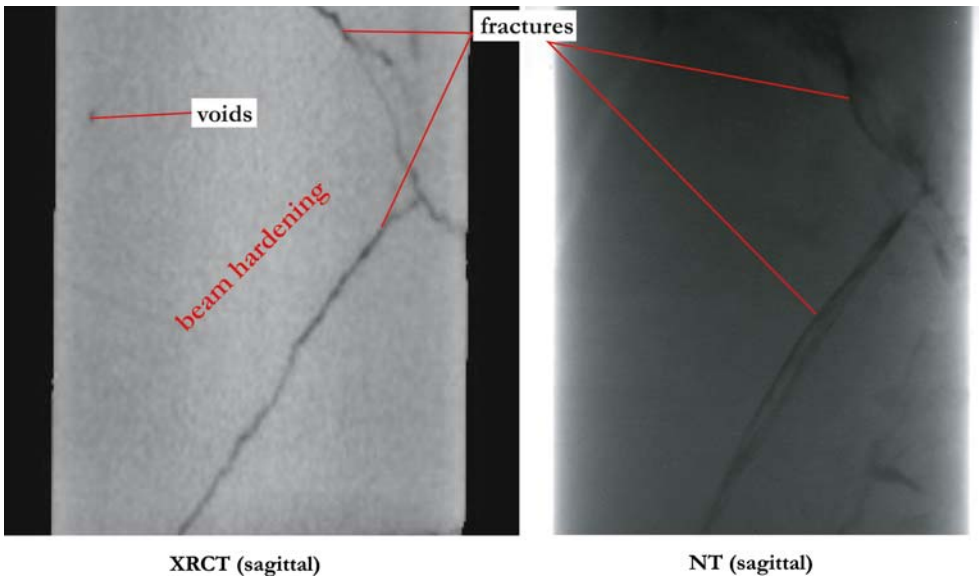

Fig. 9 Comparative sagittal XRCT (*left*) and NT slices (*right*) of sample CT4-li. XRCT slice is of medium quality, as hardening effects are visible towards central parts of the image. Calcite-filled fractures tend to be masked under X-ray investigation. The NT slice however shows more promising results in terms of structure visualization

Previous measurement tests made with medical XRCT already convinced us to properly pack the rock core sample before completion of the scan into an absorbing material that would minimize beam hardening effects. Image quality was improved considerably but very dense materials like sample CT4-li are still not artifact free. It seems that calcium, when present in strong proportion into a structure, induces some problems for proper X-ray penetration. This is particularly true when the investigated body is of the size of a geotechnical rock core. But in general, XRCT for rock investigation gives good results, as contrasting structures and textures can be visualized to a resolution of about 0.625 mm. Different components of sample CT1-co were therefore very nicely displayed on XRCT models. Problems arise with very fine-grained samples for which microstructures detection would require a finer resolution, as in the case of CT3-ma. However, apparent density contrasts inside a fine-grained matrix can be detected with XRCT and should be evaluated in terms of possible sample heterogeneity implying an eventual preferred mechanical deformation locus under stress application.

A particular weakness of XRCT is that, because it records density contrasts, features of different nature but similar densities will be masked on the resulting model. In particular, calcite-cemented fractures in sample CT4-li give a good illustration of this phenomenon.

NT investigation on borehole samples gave variable results in terms of image quality. If the proportion of hydrated mineral species is high or there is a high water content as in concrete or marl, NT scans will show almost nothing, as expected from the very high attenuation coefficient of H under neutron irradiation. This is particularly true for decimeter-scale sample sizes that are too thick for proper neutron transmission. In the case of smaller samples and smaller diameters, neutrons can give more detailed internal information that is complementary to X-ray investigation results.

On the other hand and as expressed before, if the spatial extent of hydrated minerals is comparatively low, NT tomography will provide very precise detections of H-rich zones inside the material. Sample CT4-li, consisting of a homogeneous H-poor rock matrix crossed by millimeter-wide fractures filled with hydrous minerals, would therefore be a candidate for NT investigations.

In the case of dry and H-poor samples, as is the case with CT2-sa, XRCT and NT investigations gave similar results.

For the time being, an additional advantage of XRCT is that variable volume sizes can be visualized whereas NT scan parameters as optimized for this study limit the field of view to 97 × 97 mm. Moreover, the near-parallel geometry of the neutron beam will present a persistent size-limitation in comparison to X-ray irradiation.

Acknowledgments We would like to thank Dr R. Meuli at the CHUV in Lausanne and Prof. Dr E. Lehmann at the PSI in Villigen for providing us access to the XRCT and NT scanners in the framework of this research as well as for their helpful comments during preparation of this manuscript. Dr V. Labiouse from the Laboratory of

Rock Mechanics (LMR) at the EPFL is thanked for his support in the mechanical part of the research and comments on the manuscript. Financial support for P. Christe is provided by the Swiss National Science Foundation (SNF No. 2100-63'640.00).

References

1. Berger MJ, Hubbell JH, Seltzer SM, Chang J, Coursey JS, Sukumar R, Zucker DS (1998) XCOM: photon cross sections database. National Institute of Standards and Technology, NIST Standard Reference Database 8 (XGAM)
2. Bürgi C (1999) Cataclastic fault rocks in underground excavations: a geological characterisation. Thèse EPFL GC No. 1975
3. Bürgi C, Parriaux A, Franciosi G (2001) Geological characterization of weak cataclastic fault rocks with regards to the assessment of their geomechanical properties. Q J Eng Geol Hydrogeol 34:225–232
4. Carlson WD, Denison C (1992) Mechanisms of porphyroblast crystallization: results from high-resolution computed X-ray tomography. Sciences 257:1236–1239
5. Conroy GC, Vannier MW (1984) Noninvasive three-dimensional computer imaging of matrix-filled fossil skulls by high-resolution computed tomography. Science 226:456–458
6. Habimana J (1999) Caractérisation géomécanique de roches cataclastiques rencontrées dans des ouvrages souterrains alpins. Thèse EPFL GC No. 1945
7. Habimana J, Labiouse V, Descoeudres F (2002) Geomechanical Characterisation of cataclastic rocks: experience from the Cleuson-Dixence project. Int J Rock Mech Min Sci 39:677–693
8. Hounsfield GN (1972) A method of and apparatus for examination of a body by radiation such as X- or Gamma-radiation. London, British Patent No. 1,283,915
9. Ketcham RA, Carlson WD (2001) Acquisition, optimization and interpretation of X-ray computed tomographic imagery: applications to the geosciences. Comput Geosci 27:381–400
10. Lehmann EH, Pleinert H, Wiezel L (1996) Design of a neutron radiography facility at the spallation source SINQ. Nucl Instrum Methods A377:11–15
11. Lehmann EH, Vontobel P, Wiezel L (1999) Properties of the radiography facility NEUTRA at SINQ and its potential for use as a European Reference Facility. In: Proceedings of the sixth World Conference on Neutron Radiography, Osaka, pp 151–158
12. Nakashima Y (2000) The use of X-ray CT to measure diffusion coefficients of heavy ions in water-saturated porous media. Eng Geol 56:11–17
13. Radon J (1986) On the determination of functions from their integral values along certain manifolds. IEEE Trans Med Imaging 5(4):170–176
14 Ramachandran GN, Lakshminarayanan AV (1971) Three-dimensional reconstructions from radiographs and electron micrographs: Application of convolution instead of Fourier transforms. Proc Natl Acad Sci USA 68:2236–2240
15. Schwarz D, Vontobel P, Lehmann EH, Meyer CA, Bongartz G (2005) Neutron tomography of internal structures of vertebrate remains: a comparison with X-ray computed tomography. Palaeontol Electron 8(2A):10
16. Sears VF (1992) Neutron scattering lengths and cross-sections. Neutron News 3(3):29–37
17. Van Geet M, Swennen R, Wevers M (2000) Quantitative analysis of reservoir rocks by microfocus X-ray computerized tomography. Sediment Geol 132:25–36
18. Verhelst F, Vervoort A, De Bosscher P, Marchal G (1995) X-ray computerized tomography: determination of heterogeneities in rock samples. In: Proceedings of the eighth international congress on Rock Mechanics, Sept. 25–30, 1995. Balkema, Amsterdam